Changes in interannual climate sensitivities of terrestrial carbon fluxes during the 21st century predicted by CMIP5 Earth System Models

Yongwen Liu, Tao Wang, Mengtian Huang, Yitong Yao, Philippe Ciais, Shilong Piao

AGU PUBLICATIONS

JGR

Journal of Geophysical Research: Biogeosciences

RESEARCH ARTICLE
10.1002/2015JG003124

Key Points:
- Interannual climate sensitivities of carbon fluxes from CMIP5 ESMs were analyzed
- There is a large model spread in the changes of interannual climate sensitivities of carbon fluxes
- The changes in the interannual climate sensitivity of NBP are mainly explained by those of NPP

Supporting Information:
- Supporting Information S1

Correspondence to:
S. Piao,
slpiao@pku.edu.cn

Citation:
Liu, Y., T. Wang, M. Huang, Y. Yao, P. Ciais, and S. Piao (2016), Changes in interannual climate sensitivities of terrestrial carbon fluxes during the 21st century predicted by CMIP5 Earth System Models, *J. Geophys. Res. Biogeosci.*, *121*, 903–918, doi:10.1002/2015JG003124.

Received 30 JUN 2015
Accepted 25 FEB 2016
Accepted article online 4 MAR 2016
Published online 29 MAR 2016

Changes in interannual climate sensitivities of terrestrial carbon fluxes during the 21st century predicted by CMIP5 Earth System Models

Yongwen Liu[1], Tao Wang[2,3], Mengtian Huang[1], Yitong Yao[1], Philippe Ciais[4], and Shilong Piao[1,2,3]

[1]Sino-French Institute for Earth System Science, College of Urban and Environmental Sciences, Peking University, Beijing, China, [2]Key Laboratory of Alpine Ecology and Biodiversity, Institute of Tibetan Plateau Research, Chinese Academy of Sciences, Beijing, China, [3]CAS Center for Excellence in Tibetan Plateau Earth Sciences, Chinese Academy of Sciences, Beijing, China, [4]LSCE, UMR CEA-CNRS, Gif-sur-Yvette, France

Abstract Terrestrial carbon fluxes are sensitive to climate change, but the interannual climate sensitivity of the land carbon cycle can also change with time. We analyzed the changes in responses of net biome production (NBP), net primary production (NPP), and heterotrophic respiration (Rh) to interannual climate variations over the 21st century in the Earth System Models (ESMs) from the Coupled Model Intercomparison Project 5. Under Representative Concentration Pathway (RCP) 4.5, interannual temperature sensitivities of NBP (γ_{NBP}^{Temp}), NPP (γ_{NPP}^{Temp}), and Rh (γ_{Rh}^{Temp}) remain relatively stable at global scale, yet with large differences among ESMs and spatial heterogeneity. Modeled γ_{NPP}^{Temp} and γ_{Rh}^{Temp} appear to increase in parallel in boreal regions, resulting in unchanged γ_{NBP}^{Temp}. Tropical γ_{NBP}^{Temp} decreases in most models, due to decreasing γ_{NPP}^{Temp} and relatively stable γ_{Rh}^{Temp}. Across models, the changes in γ_{NBP}^{Temp} can be mainly explained by changes in γ_{NPP}^{Temp} rather than changes in γ_{Rh}^{Temp}, at both global and regional scales. Interannual precipitation sensitivities of global NBP (γ_{NBP}^{Prec}), NPP (γ_{NPP}^{Prec}), and Rh (γ_{Rh}^{Prec}) are predicted not to change significantly, with large differences among ESMs. Across models, the changes in γ_{NBP}^{Prec} can be mainly explained by changes in γ_{NPP}^{Prec} rather than changes in γ_{Rh}^{Prec} in temperate regions, but not in other regions. Changes in the interannual climate sensitivities of carbon fluxes are consistent across RCPs 4.5, 6.0, and 8.5 but larger in more intensive scenarios. More effort should be considered to improve terrestrial carbon flux responses to interannual climate variability, e.g., incorporating biogeochemical processes of nutrient limitation, permafrost dynamics, and microbial decomposition.

1. Introduction

Interannual variation in the annual growth rate of atmospheric CO_2 is related to the variation in terrestrial ecosystem carbon fluxes, due to responses of ecological processes to interannual climate variability, e.g., temperature and precipitation [*Schneising et al.*, 2014; *Zeng et al.*, 2005]. Recently, *Cox et al.* [2013] found that the observed interannual variability in the growth rate of atmospheric CO_2 was linearly correlated with the interannual variability in the tropical temperature during the past 50 years (1960–2010). The observed interannual sensitivity of the annual CO_2 growth rate to tropical interannual temperature anomalies in the period 1960–2010 (5.1 ± 0.9 Pg C year^{-1} K^{-1}), was used to constrain the long-term (1960–2099) sensitivity of tropical land carbon stocks to climate change (53 ± 17 Pg C K^{-1}), based an emergent relationship between past interannual and future long-term sensitivities across climate-carbon cycle models [*Cox et al.*, 2013]. Some correlation between short- and long-term climate sensitivities can be expected if both short- and long-term responses of tropical ecosystems to climate change are driven by similar processes in models, e.g., the impact of climate change on the balance of carbon fluxes in tropics. This correlation only holds if the model structure is "simple," but it would not be valid in presence of nonlinear response of net primary production (NPP) to climate change, nutrient limitation, forest "dieback" [*Cox et al.*, 2004], priming effects on decomposition [*Guenet et al.*, 2013], or microbial changes in decomposition [*Wieder et al.*, 2013]. Thus, the interannual climate sensitivity of carbon flux in the past 50 years may not be related to the long-term climate sensitivity of carbon flux (e.g., 1960–2099) unless the responses of carbon flux to interannual climate variability will remain roughly proportional to the response under future climate change scenarios.

The interannual climate sensitivity of terrestrial net carbon flux appears to change with time [*Wang et al.*, 2014], depending on the different responses of terrestrial NPP and heterotrophic respiration (Rh) to interannual

climate variations. In temperate and Arctic ecosystems of the Northern Hemisphere, the strength of the interannual correlation between NPP and temperature declined substantially over the last three decades, possibly due to an increase in drought in the temperate ecosystems and a nonlinear response of photosynthesis to temperature in the Arctic ecosystems [*Piao et al*., 2014]. In a semiarid region like Australia, multiple lines of evidence demonstrate that the sensitivity of continental net carbon uptake to precipitation variations has increased during the last three decades [*Poulter et al*., 2014]. The responses of Rh to interannual climate variability are mainly dependent upon temperature and soil/litter carbon pools (mainly the labile ones) available for decomposition [*Bond-Lamberty and Thomson*, 2010]. Predicted both global temperature and soil carbon show increase trend during the 21st century [*Todd-Brown et al*., 2014] and therefore likely result in changing interannual climate sensitivity of Rh in the future.

Besides temporal heterogeneity, the interannual climate sensitivities of terrestrial carbon fluxes also have spatial heterogeneity varying with ecohydrologic conditions. The variations in CO_2 growth rate appears to be mainly dominated by the responses of tropical carbon fluxes to temperature variations [*Cox et al*., 2013; *Wenzel et al*., 2014]. Subtropical ecosystems are also regarded as mainly contributing to variability of the global land CO_2 flux, e.g., semiarid vegetation in the Southern Hemisphere, where high precipitation can produce a strong carbon uptake during wet years such as during the 2010–2012 La Niña episodes [*Ahlström et al*., 2015; *Bastos et al*., 2013; *Poulter et al*., 2014]. In middle and high latitudes of the Northern Hemisphere where ecosystems can be limited both by water and temperature during different seasons, anomalies of net CO_2 flux can be affected by the interactions between changes in temperature and precipitation [*Angert et al*., 2005; *Poulter et al*., 2013]. In addition, fire emissions of CO_2 also contribute to the interannual variations of CO_2 growth rate but they seem to have a smaller contribution than NPP and Rh anomalies at hemispheric scale [*van der Werf et al*., 2010].

To examine whether interannual climate sensitivities of terrestrial carbon flux will change during the 21st century, we investigate changes in the responses of land carbon flux to climate variations on the interannual timescale over the 21st century from Earth System Models (ESMs) participating in the fifth phase of the Coupled Model Intercomparison Project (CMIP5). Considering the spatial heterogeneity of interannual climate sensitivities of terrestrial carbon flux, changes in the sensitivities at both global and regional scales are analyzed in this study. Specifically, we aimed to (1) compare changes in the responses of terrestrial ecosystems net carbon flux to interannual climate variations across ESMs at both global and regional scales and (2) identify which carbon flux component, NPP or Rh, leads to the changes in interannual climate sensitivities of net carbon flux across ESMs.

2. Material and Methods

2.1. Earth System Models in CMIP5

In this study, we used CMIP5 ESMs simulations contributed to the Intergovernmental Panel on Climate Change Fifth Assessment Report (AR5) [*Taylor et al*., 2012]. Two types of CMIP5 long-term experiments: historical simulations (1850–2005) and future projections (2006–2100) were analyzed. For the 21st century, we use future projection simulations from ESMs forced with four specified concentrations referred to as "Representative Concentration Pathways" (RCPs) that are based on a range of projections of future population growth, technologies development, and societal responses. There are four pathways RCP2.6, RCP4.5, RCP6.0, and RCP8.5 representing different future CO_2 and radiative forcing scenarios from low to high, respectively [*Jones et al*., 2013; *van Vuuren et al*., 2011b]. RCP2.6 is a low emission scenario, with a peak in radiative forcing at ~3 W m^{-2} (~443 ppm CO_2) at 2050 and then a decline to 2.6 W m^{-2} (~421 ppm CO_2) near the end of the 21st century [*van Vuuren et al*., 2011a]. RCP4.5 is a medium-low emission scenario, which stabilizes radiative forcing at 4.5 W m^{-2} (~538 ppm CO_2) in the year 2100 [*Thomson et al*., 2011]. RCP6.0 is a medium-high emission scenario, which describes a stabilization pathway to 6.0 W m^{-2} (~670 ppm CO_2) [*Masui et al*., 2011]. RCP8.5 assumes a high-emission scenario with no mitigation, with a radiative forcing increasing up to 8.5 W m^{-2} in 2100 (~936 ppm CO_2) by 2100 [*Riahi et al*., 2011]. Over the 21st century, all ESMs predict that global temperatures continue to rise under all RCPs. Relative to the period 1986–2005, global mean surface temperatures increase by on average 1.0°C, 1.8°C, 2.2°C, and 3.7°C under RCPs 2.6, 4.5, 6.0, and 8.5 during the period 2081–2100, respectively [*Collins et al*., 2013].

Monthly outputs of CMIP5 ESMs were downloaded from the Program for Climate Model Diagnosis and Intercomparison (PCMDI) server: Earth System Grid Federation [*Cinquini et al*., 2014] (http://cmip-pcmdi.llnl.gov/cmip5). As shown in Table S1 in the supporting information, 17 fully coupled ESMs from CMIP5 were used in this analysis, that have both historical ("historical" experiment) and future RCPs simulations for net biome production (NBP), NPP, Rh, air temperature, precipitation, and surface downwelling shortwave radiation variables (nbp, npp, rh, tas, pr, and rsds, respectively, from the CMIP5 variable list). Not every ESM ran all RCP pathways. All 17 CMIP5 ESMs have historical simulations, but among the 17 models, the number of ESMs having RCPs 2.6, 4.5, 6.0, and 8.5 runs is 12, 16, 9, and 17, respectively (Table S1). Except for CanESM2, HadGEM2-CC, HadGEM2-ES, MIROC-ESM, and MIROC-ESM-CHEM, the other 12 models in Table S1 have considered the interactive effects of fires. Furthermore, three ESMs (BNU-ESM, CESM1-BGC, and NorESM1-ME) have an explicit representation of interactive carbon-nitrogen (C-N) cycle, but the C-N cycle interaction in BNU-ESM was turned off in the CMIP5 simulations [*Ji et al*., 2014].

Table S1 shows the ensemble number of each model under each scenario. Across scenarios, the ensemble number was not identical for several models, e.g., CCSM4, HadGEM2-CC, HadGEM2-ES, IPSL-CM5A-LR, MIROC-ESM, MPI-ESM-MR, NorESM1-M, and NorESM1-ME (Table S1). For each model under each individual scenario, if multiple ensembles were available, all ensembles of output were averaged following previous studies [*Todd-Brown et al*., 2013, 2014]. Thus, the simulation results under each scenario for each model were presented as the averaged multiple ensembles, rather than any one specific ensemble. The average of ensemble members might reduce the variability and most of models have different number of realizations between historical simulations and future projections that may artificially induce the inconsistency in variability. To understand whether this could affect our results, we have also performed analyses based on a single realization r1i1p1, since which was produced by all 16 models under both historical and RCP4.5 scenarios. Our results have shown that the conclusions based on this single realization (Figures S1–S4) were similar with those based on the average of all realizations (Figures 1–4). All ESMs outputs are regridded to $1° \times 1°$ using the first-order conservative remapping scheme [*Jones*, 1999], as implemented by Climate Data Operators (https://code.zmaw.de/projects/cdo). In addition, we limited our study region to the vegetated land area that is defined as all grid points for which the mean annual normalized difference vegetation index (NDVI) during 1982–2009 was larger than 0.1. The NDVI data were obtained from the Global Inventory Monitoring and Modelling Studies (GIMMS) group, and the third generation GIMMS NDVI from advanced very high resolution radiometer sensors (NDVI3g) was used in this study [*Pinzon and Tucker*, 2014]. Please note that the vegetated land area defined by NDVI may be not fully consistent with that in model simulations.

2.2. Analysis

We analyzed the responses of NBP, NPP, and Rh to the interannual variability of climate factors (annual temperature, precipitation, and surface downwelling shortwave radiation) during 1975–2004 (historical simulation) and 2069–2098 (RCPs 2.6, 4.5, 6.0, and 8.5 simulations) in CMIP5 ESMs. In each period, the interannual climate sensitivities were diagnosed using a multiple regression approach:

$$y = \gamma^{\mathrm{Temp}} x_{\mathrm{T}} + \gamma^{\mathrm{Prec}} x_{\mathrm{P}} + \gamma^{\mathrm{Radi}} x_{\mathrm{R}} + \varepsilon, \tag{1}$$

where

y is the detrended anomaly of carbon flux: NBP, NPP, or Rh;
x_{T} is the detrended anomaly of air temperature (tas);
x_{P} is the detrended anomaly of precipitation (pr);
x_{R} is the detrended anomaly of surface downwelling shortwave radiation (rsds);
γ^{Temp}, γ^{Prec}, and γ^{Radi} are the apparent carbon flux sensitivities to interannual variations in temperature, precipitation, and radiation, respectively [*Piao et al*., 2013]. The word "apparent" means the partial derivative with regard to the change of a given climate factor, whereas in the real world, these factors covary; and
ε is the residual error term. Changes in γ^{Temp}, γ^{Prec}, and γ^{Radi} during the 21st century (period 2069–2098 minus period 1975–2004) is denoted by $\Delta\gamma^{\mathrm{Temp}}$, $\Delta\gamma^{\mathrm{Prec}}$, and $\Delta\gamma^{\mathrm{Radi}}$, respectively, in the following text.

We analyzed both spatial patterns and regional values of the apparent carbon flux sensitivities to interannual climate variations. When analyzing spatial distributions, carbon and climate variables in each grid cell were used

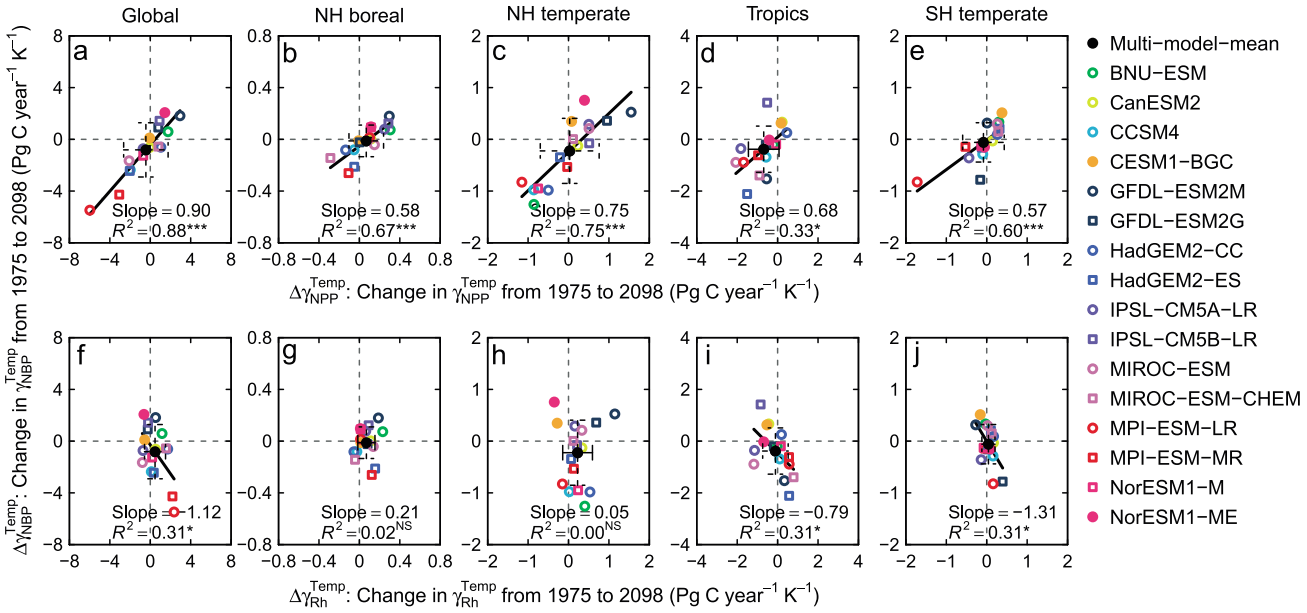

Figure 1. Changes in global and regional sensitivities of net biome production (NBP), net primary production (NPP), and heterotrophic respiration (Rh) to interannual temperature variations under RCP4.5 ($\Delta\gamma^{Temp}_{NBP}$, $\Delta\gamma^{Temp}_{NPP}$, and $\Delta\gamma^{Temp}_{Rh}$). γ^{Temp}_{NBP}, γ^{Temp}_{NPP}, and γ^{Temp}_{Rh} are estimated using equation (1). $\Delta\gamma^{Temp}_{NBP}$, $\Delta\gamma^{Temp}_{NPP}$, and $\Delta\gamma^{Temp}_{Rh}$ are calculated as the difference of γ^{Temp}_{NBP}, γ^{Temp}_{NPP}, and γ^{Temp}_{Rh} between the periods 2069–2098 (RCP4.5 runs) and 1975–2004 (historical simulations). Multimodel means are shown as black points with the whiskers representing the standard deviation. Dashed error bar indicates the multimodel mean is statistically insignificant ($P > 0.05$). Significant differences of simple regression analysis are reported as ^{NS}, $P > 0.05$; *, $P < 0.05$; **, $P < 0.01$; and ***, $P < 0.001$.

to calculate interannual climate sensitivities of carbon fluxes. When analyzing regional results, we aggregated each output variable of each model over the following latitudinal bands: Northern Hemisphere boreal regions (50°N–90°N), Northern Hemisphere temperate (NH temperate) (23°N–50°N), tropics (23°S–23°N), Southern Hemisphere temperate (SH temperate) (23°S–50°S), and the entire globe. Then, regional interannual climate sensitivities of carbon fluxes were calculated using the regional-aggregate variables. We did not average the slope across latitude bands but aggregated the grids by latitude and then calculated the slope using equation (1). The statistical significance of projected changes in multimodel mean of apparent carbon flux sensitivities to interannual climate variations were examined using a Wilcoxon signed-ranked test, following a previous study [*Collins et al*., 2013].

Please note that the ESMs are not completely independent. Some of models share the same land scheme but differ in atmosphere or ocean components. For example, the only difference between GFDL-ESM2M and GFDL-ESM2G is the ocean module. CESM1-BGC and NorESM1-ME used the same land surface scheme of CLM4 (Community Land Model version 4) but used different ocean and atmospheric components. Model discrepancy in ocean and atmospheric components can result in the differences in precipitation and land surface temperatures, which further impact carbon fluxes and their sensitivities to interannual climate change (the main finding of this paper; the sensitivities could change in the temporal scale). Therefore, in this study, we did not average the simulations of the ESM with same land surface scheme so as not to exclude other factors that might influence the interannual climate sensitivities of terrestrial carbon fluxes (such as a different climate model). Nevertheless, the model simulations are not totally independent especially for ESMs with the same land surface scheme. The statistical tests based on those simulations therefore should be interpreted carefully. In the following sections, changes in carbon fluxes apparent sensitivities to interannual climate variations under RCP4.5 are expressed as examples, and changes in interannual climate sensitivities of carbon fluxes under RCPs 2.6, 6.0, and 8.5 are shown in the supporting information.

3. Results

3.1. Changes in Apparent Sensitivities of Carbon Fluxes to Interannual Temperature Variations ($\Delta\gamma^{Temp}$)

Under RCP4.5, at the global scale, predicted multimodel mean $\Delta\gamma^{Temp}_{NBP}$, $\Delta\gamma^{Temp}_{NPP}$, and $\Delta\gamma^{Temp}_{Rh}$ are nonsignificant but vary widely across models (Figures 1a and 1f; specific values in Figure 1 were listed in Table S2). MPI-ESM-LR has

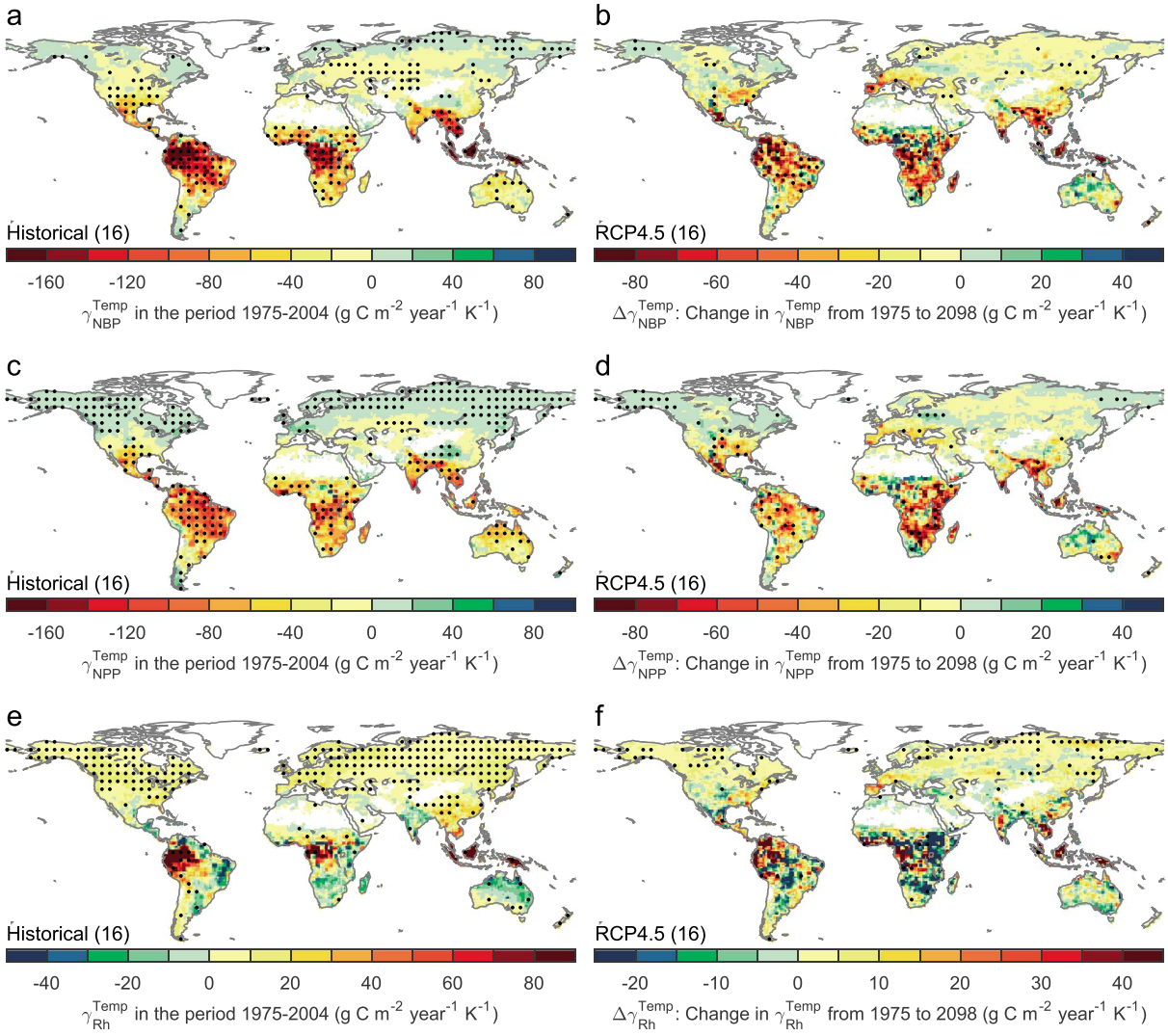

Figure 2. Spatial distributions of multimodel mean γ^{Temp}_{NBP}(a), γ^{Temp}_{NPP}(c), and γ^{Temp}_{Rh}(e), and their changes from 1975 to 2098 under RCP4.5 ($\Delta\gamma^{Temp}_{NBP}$(b), $\Delta\gamma^{Temp}_{NPP}$(d), and $\Delta\gamma^{Temp}_{Rh}$(f)). γ^{Temp}_{NBP}, γ^{Temp}_{NPP}, and γ^{Temp}_{Rh} are estimated using equation (1). $\Delta\gamma^{Temp}_{NBP}$, $\Delta\gamma^{Temp}_{NPP}$, and $\Delta\gamma^{Temp}_{Rh}$ are estimated as the difference of γ^{Temp}_{NBP}, γ^{Temp}_{NPP}, and γ^{Temp}_{Rh} between the periods 2069–2098 (RCP4.5 runs) and 1975–2004 (historical simulations). Black point signs indicate grid points where the multimodel mean changes are significant at the 5% level using a Wilcoxon signed-ranked test. Models used: BNU-ESM, CanESM2, CCSM4, CESM1-BGC, GFDL-ESM2M, GFDL-ESM2G, HadGEM2-CC, HadGEM2-ES, IPSL-CM5A-LR, IPSL-CM5B-LR, MIROC-ESM, MIROC-ESM-CHEM, MPI-ESM-LR, MPI-ESM-MR, NorESM1-M, and NorESM1-ME.

the largest decrease in γ^{Temp}_{NBP} of -5.47 Pg C year^{-1} K^{-1}, probably due to its largest decrease in γ^{Temp}_{NPP} and highest increase in γ^{Temp}_{Rh} among all models (Figures 1a and 1f). NorESM1-ME shows the largest positive $\Delta\gamma^{Temp}_{NBP}$ of 2.07 Pg C year^{-1} K^{-1}, probably because of its positive $\Delta\gamma^{Temp}_{NPP}$ and negative $\Delta\gamma^{Temp}_{Rh}$ (Figures 1a and 1f). Across models, $\Delta\gamma^{Temp}_{NBP}$ is positively correlated with $\Delta\gamma^{Temp}_{NPP}$ ($R^2 = 0.88$, $P < 0.001$) (Figure 1a) but negatively correlated with $\Delta\gamma^{Temp}_{Rh}$ ($R^2 = 0.31$, $P = 0.03$) (Figure 1f). Differences between models in $\Delta\gamma^{Temp}_{NBP}$ are mainly explained by the differences in $\Delta\gamma^{Temp}_{NPP}$ (Figure 1a), rather than by the differences in $\Delta\gamma^{Temp}_{Rh}$ (Figure 1f). The same NPP dominance holds true for RCP2.6 (Figure S5), RCP6.0 (Figure S6), and RCP8.5 (Figure S7).

In most ESMs, γ^{Temp}_{NBP} is spatially heterogeneous, with negative values in tropical regions, but positive values in high latitudes (Figures 2a and S8a–S10a). However, predicted multimodel mean $\Delta\gamma^{Temp}_{NBP}$ under RCP4.5 are nonsignificant over most of the globe (Figures 1 and 2b; Projections of $\Delta\gamma^{Temp}_{NBP}$ by each individual ESM under all RCPs are shown in Figures S11–S14). In the boreal zone and NH temperate regions, nonsignificant $\Delta\gamma^{Temp}_{NBP}$ and $\Delta\gamma^{Temp}_{NPP}$ are diagnosed (Figure 1), in contrast with significantly positive $\Delta\gamma^{Temp}_{Rh}$ with multimodel mean of 0.07 ± 0.08 Pg C year^{-1} K^{-1} ($P = 0.008$) and 0.22 ± 0.37 Pg C year^{-1} K^{-1} ($P = 0.03$), respectively (Figure 1). Boreal $\Delta\gamma^{Temp}_{NBP}$ ranges from -0.26 Pg C year^{-1} K^{-1} (MPI-ESM-MR) to 0.18 Pg C year^{-1} K^{-1}

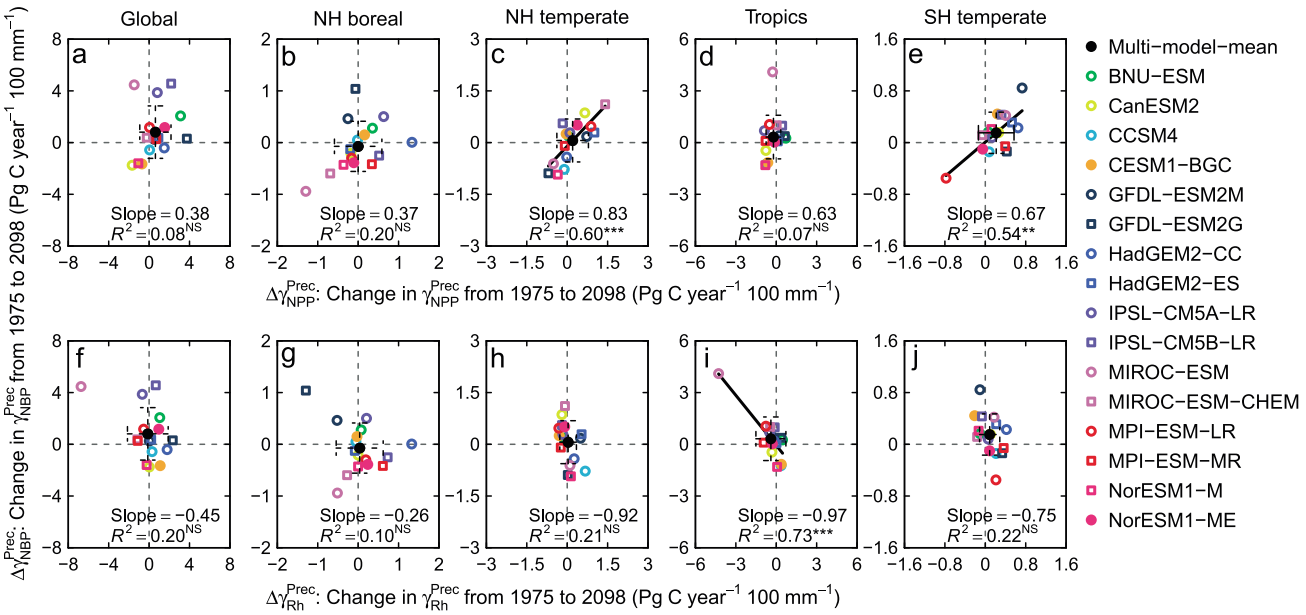

Figure 3. Changes in global and regional sensitivities of NBP, NPP, and Rh to interannual precipitation variations under RCP4.5 ($\Delta\gamma^{Prec}_{NBP}$, $\Delta\gamma^{Prec}_{NPP}$, and $\Delta\gamma^{Prec}_{Rh}$). γ^{Prec}_{NBP}, γ^{Prec}_{NPP}, and γ^{Prec}_{Rh} are estimated using equation (1). $\Delta\gamma^{Prec}_{NBP}$, $\Delta\gamma^{Prec}_{NPP}$, and $\Delta\gamma^{Prec}_{Rh}$ are estimated as the difference of γ^{Prec}_{NBP}, γ^{Prec}_{NPP}, and γ^{Prec}_{Rh} between the periods 2069–2098 (RCP4.5 runs) and 1975–2004 (historical simulations). Multimodel means are shown as black points with the whiskers representing the standard deviation. Dashed error bar indicates the multimodel mean is statistically insignificant ($P > 0.05$). Significant differences of simple regression analysis are reported ^{NS}, $P > 0.05$; *, $P < 0.05$; **, $P < 0.01$; and ***, $P < 0.001$.

(GFDL-ESM2M) (Figure 1b). Across models, $\Delta\gamma^{Temp}_{NBP}$ is mainly explained by $\Delta\gamma^{Temp}_{NPP}$, rather than $\Delta\gamma^{Temp}_{Rh}$ in both boreal and NH temperate regions (Figure 1).

In tropical regions, most models (12 of 16 models) have negative $\Delta\gamma^{Temp}_{NBP}$, although with a nonsignificant multimodel mean (Figure 1d). Tropical $\Delta\gamma^{Temp}_{NBP}$ ranges from −2.11 Pg C year^{-1} K^{-1} (HadGEM2-ES) to 1.42 Pg C year^{-1} K^{-1} (IPSL-CM5B-LR) (Figure 1d). Under all RCPs, ESMs predict significantly negative $\Delta\gamma^{Temp}_{NPP}$ (Figures 1d and S5d–S7d), but not significant $\Delta\gamma^{Temp}_{Rh}$ (Figures 1i, S5i–S7i). Cross-model differences in $\Delta\gamma^{Temp}_{NBP}$ can be mainly explained by both $\Delta\gamma^{Temp}_{NPP}$ and $\Delta\gamma^{Temp}_{Rh}$ under RCP4.5 (Figures 1d and 1i) but by $\Delta\gamma^{Temp}_{Rh}$ under RCP2.6 (Figures S5d and S5i) and by $\Delta\gamma^{Temp}_{NPP}$ under RCP8.5 (Figures S7d and S7i).

In the SH temperate regions, predicted $\Delta\gamma^{Temp}_{NBP}$ ranges from −0.82 Pg C year^{-1} K^{-1} (MPI-ESM-LR) to 0.51 Pg C year^{-1} K^{-1} (CESM1-BGC), with a nonsignificant multimodel mean (Figure 1e). MPI-ESM-LR predicts the largest decline of γ^{Temp}_{NBP}, likely due to its largest decrease of γ^{Temp}_{NPP} (Figure 1e). GFDL-ESM2G shows a comparable change in γ^{Temp}_{NBP} (−0.78 Pg C year^{-1} K^{-1}) (Figure 1e) but probably partly because of a relatively high $\Delta\gamma^{Temp}_{Rh}$ (Figure 1j). Intermodel differences in $\Delta\gamma^{Temp}_{NBP}$ in SH temperate regions can be explained by both differences in $\Delta\gamma^{Temp}_{NPP}$ ($R^2 = 0.60$, $P < 0.001$) and differences in $\Delta\gamma^{Temp}_{Rh}$ ($R^2 = 0.31$, $P = 0.02$) under RCP4.5 (Figures 1e and 1j).

3.2. Changes in Apparent Sensitivities of Carbon Fluxes to Interannual Precipitation Variations ($\Delta\gamma^{Prec}$)

At the global scale, $\Delta\gamma^{Prec}_{NBP}$ ranges from −1.75 Pg C year^{-1} 100 mm^{-1} (CanESM2) to 4.56 Pg C year^{-1} 100 mm^{-1} (IPSL-CM5B-LR), with a nonsignificant multimodel mean (Figure 3a; specific values in Figure 3 were listed in Table S3). Across all models, $\Delta\gamma^{Prec}_{NBP}$ is not significantly correlated with $\Delta\gamma^{Prec}_{NPP}$ or $\Delta\gamma^{Prec}_{Rh}$ under RCP 4.5 (Figures 3a and 3f) but is mainly explained by $\Delta\gamma^{Prec}_{NPP}$ under RCP2.6 (Figure S15a) and RCP8.5 (Figure S17a).

In most ESMs, γ^{Prec}_{NBP} is spatially heterogeneous, with positive values over the most of globe (except in the northern part of the boreal band) (Figures 4a and S18a–S20a). However, nonsignificant $\Delta\gamma^{Prec}_{NBP}$ under RCP4.5 is globally distributed (Figure 4b; projections of $\Delta\gamma^{Prec}_{NBP}$ by each individual ESM are shown in Figures S21–S24). In boreal regions, 9 of 16 models predict negative $\Delta\gamma^{Prec}_{NBP}$ but with a nonsignificant multimodel mean (Figure 3b). Boreal $\Delta\gamma^{Prec}_{NBP}$ ranges from −0.94 Pg C year^{-1} 100 mm^{-1} (MIROC-ESM) to 1.04 Pg C year^{-1} 100 mm^{-1} (GFDL-ESM2G) (Figure 3b). Both multimodel mean values of $\Delta\gamma^{Prec}_{NPP}$ and $\Delta\gamma^{Prec}_{Rh}$ in boreal regions are close to zero (Figures 3b and 3g). Cross-model differences in $\Delta\gamma^{Prec}_{NBP}$ are mainly

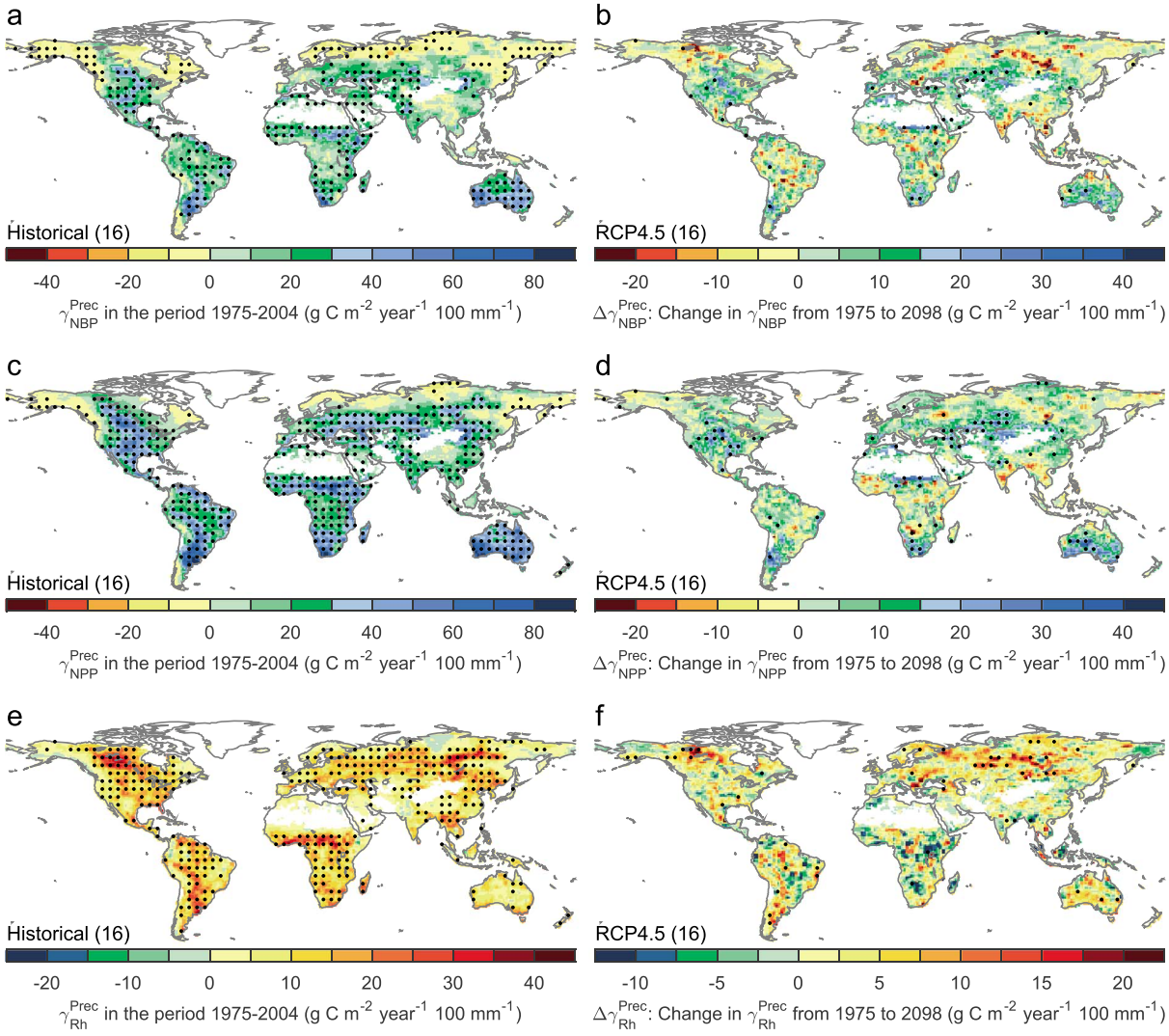

Figure 4. Spatial distributions of multimodel mean γ^{Prec}_{NBP} (a), γ^{Prec}_{NPP} (c), and γ^{Prec}_{Rh} (e), and their changes from 1975 to 2098 under RCP4.5 ($\Delta\gamma^{Prec}_{NBP}$, (b), $\Delta\gamma^{Prec}_{NPP}$, (d), and $\Delta\gamma^{Prec}_{Rh}$) (f). γ^{Prec}_{NBP}, γ^{Prec}_{NPP}, and γ^{Prec}_{Rh} are estimated using equation (1). $\Delta\gamma^{Prec}_{NBP}$, $\Delta\gamma^{Prec}_{NPP}$, and $\Delta\gamma^{Prec}_{Rh}$ are estimated as the difference of γ^{Prec}_{NBP}, γ^{Prec}_{NPP}, and γ^{Prec}_{Rh} between the periods 2069–2098 (RCP4.5 runs) and 1975–2004 (historical simulations). Black point signs indicate grid points where the multimodel mean changes are significant at the 5% level using a Wilcoxon signed-ranked test. Models used: BNU-ESM, CanESM2, CCSM4, CESM1-BGC, GFDL-ESM2M, GFDL-ESM2G, HadGEM2-CC, HadGEM2-ES, IPSL-CM5A-LR, IPSL-CM5B-LR, MIROC-ESM, MIROC-ESM-CHEM, MPI-ESM-LR, MPI-ESM-MR, NorESM1-M, and NorESM1-ME.

explained by $\Delta\gamma^{Prec}_{NPP}$ under RCP2.6 and RCP 6.0 (Figures S15 and S16) but are nonsignificantly correlated with differences in $\Delta\gamma^{Prec}_{NPP}$ or $\Delta\gamma^{Prec}_{Rh}$ under RCP4.5 and RCP8.5 (Figures 3 and S17).

In NH temperate regions, $\Delta\gamma^{Prec}_{NBP}$ ranges from -0.93 Pg C year^{-1} 100 mm^{-1} (NorESM1-M) to 1.11 Pg C year^{-1} 100 mm^{-1} (MIROC-ESM-CHEM), with 10 of 16 models predicting positive $\Delta\gamma^{Prec}_{NBP}$ (Figure 3c). Across models, variations in $\Delta\gamma^{Prec}_{NBP}$ are significantly correlated with variations in $\Delta\gamma^{Prec}_{NPP}$ under all RCPs (Figures 3c and S15c–S17c) but are not significantly correlated with variations in $\Delta\gamma^{Prec}_{Rh}$ under most RCPs (except RCP2.6) (Figures 3h and S15h–S17h). Thus, in NH temperate regions, differences in $\Delta\gamma^{Prec}_{NBP}$ across models mainly depend on differences in $\Delta\gamma^{Prec}_{NPP}$ rather than differences in $\Delta\gamma^{Prec}_{Rh}$. For example, in the southern United States and central Asia, CMIP5 ESMs show consistency across models for an increase in γ^{Prec}_{NPP} under RCP4.5 (Figure 4d), resulting in positive $\Delta\gamma^{Prec}_{NBP}$ values (Figure 4b). The patterns of $\Delta\gamma^{Prec}_{NBP}$ in NH temperate regions are consistent across RCPs 4.5, 6.0, and 8.5 (Figures 4b, S19b, and S20b).

In the tropics, $\Delta\gamma^{Prec}_{NBP}$ has a nonsignificant multimodel mean but vary widely across models (Figure 3d). MIROC-ESM has the highest $\Delta\gamma^{Prec}_{NBP}$ (4.10 Pg C year^{-1} 100 mm^{-1}), probably due to its largest decline in γ^{Prec}_{Rh} (-4.28 Pg C year^{-1}

100 mm^{-1}) (Figure 3i). NorESM1-M simulates the largest decrease in γ_{NBP}^{Prec} (−1.31 Pg C year^{-1} 100 mm^{-1}), probably because of its largest decrease in γ_{NPP}^{Prec} (−0.81 Pg C year^{-1} 100 mm^{-1}) (Figure 3d). Across all models, $\Delta\gamma_{NBP}^{Prec}$ is not correlated with $\Delta\gamma_{NPP}^{Prec}$ under all RCPs (Figures 3d and S15d–S17d) and significantly correlated with $\Delta\gamma_{Rh}^{Prec}$ only under RCP4.5 (Figures 3i and S15i–S17i).

In SH temperate regions, diagnosed $\Delta\gamma_{NBP}^{Prec}$ under RCP4.5 ranges from −0.55 Pg C year^{-1} 100 mm^{-1} (MPI-ESM-LR) to 0.85 Pg C year^{-1} 100 mm^{-1} (GFDL-ESM2M), with a multimodel mean of 0.15 ± 0.32 Pg C year^{-1} 100 mm^{-1} (P = 0.051) (Figure 3e). Across models, γ_{NPP}^{Prec} increases over the 21st century, with a significant multimodel mean $\Delta\gamma_{NPP}^{Prec}$ of 0.22 ± 0.35 Pg C year^{-1} 100 mm^{-1} (P = 0.009) (Figure 3e). Different from $\Delta\gamma_{NPP}^{Prec}$, predicted $\Delta\gamma_{Rh}^{Prec}$ is not significant (Figure 3j). Under all RCPs, cross-model differences in $\Delta\gamma_{NBP}^{Prec}$ are significantly correlated with differences in $\Delta\gamma_{NPP}^{Prec}$ (Figures 3e and S15e-S17e), but not significantly correlated with differences in $\Delta\gamma_{Rh}^{Prec}$ (Figures 3j and S15j–S17j). Hence, differences in SH temperate $\Delta\gamma_{NBP}^{Prec}$ across models mainly depend on differences in $\Delta\gamma_{NPP}^{Prec}$ instead of differences in $\Delta\gamma_{Rh}^{Prec}$.

Besides changes in γ^{Temp} and γ^{Prec}, changes in γ^{Radi} during the 21st century were analyzed and are shown in the supporting information (Figures S25–S36). During the 21st century, the multimodel mean γ_{NBP}^{Radi} remains relatively stable at both global and regional scales, yet with a large model spread. Cross-model differences in $\Delta\gamma_{NBP}^{Radi}$ are significantly correlated with differences in $\Delta\gamma_{NPP}^{Radi}$, but not significantly correlated with difference in $\Delta\gamma_{Rh}^{Radi}$. Overall, predicted changes in the apparent sensitivities of NBP, NPP, and Rh to interannual variations in temperature, precipitation, and radiation during the 21st century vary strongly across ESMs at both global and regional scales.

4. Discussion

4.1. Change in Apparent Sensitivity of Tropical Net Biome Productivity to Interannual Temperature Variations in the Past Five Decades

The variation in growth of atmospheric CO_2 was considered to be mainly dominated by the responses of tropical ecosystems net carbon flux to temperature variations [*Cox et al*., 2013; *Wenzel et al*., 2014]. *Wang et al*. [2014] found that the sensitivity of atmospheric CO_2 growth rate to interannual tropical temperature variability has increased from 2.6 ± 0.5 Pg C year^{-1} K^{-1} to 4.8 ± 1.0 Pg C year^{-1} K^{-1} between 1960–1979 and 1992–2011. This positive temperature sensitivity of the atmospheric growth rate corresponds to a negative sensitivity of the tropical terrestrial biosphere. This indicates that tropical γ_{NBP}^{Temp} declined by a factor of 2 during past five decades [*Wang et al*., 2014]. Herein, Figure 5 shows the changes in tropical γ_{NBP}^{Temp} across CMIP5 ESMs during the period 1955–2004. In the early time widow (1955–1979), 13 of 17 ESMs (except for CCSM4, CESM1-BGC, IPSL-CM5B-LR, and NorESM1-M) have significant negative values of tropical γ_{NBP}^{Temp}, ranging from −1.24 Pg C year^{-1} K^{-1} (NorESM1-ME) to −4.94 Pg C year^{-1} K^{-1} (MRI-ESM1) (Figure 5a). In the recent time window (1980–2004), 15 of 17 ESMs (except for CCSM4 and NorESM1-M) have significant negative values of tropical γ_{NBP}^{Temp}, ranging from −1.20 Pg C year^{-1} K^{-1} (CESM1-BGC) to −4.48 Pg C year^{-1} K^{-1} (HadGEM2-CC) (Figure S37). However, only one ESM (IPSL-CM5B-LR) produced a relatively large decrease in γ_{NBP}^{Temp}, from −1.06 Pg C year^{-1} K^{-1} (1955–1979) to −3.23 Pg C year^{-1} K^{-1} (1980–2004) (Figure 5b). During the past five decades (period 1980–2004 minus period 1955–1979), $\Delta\gamma_{NBP}^{Temp}$, $\Delta\gamma_{NPP}^{Temp}$, and $\Delta\gamma_{Rh}^{Temp}$ are not consistent between models, and the multimodel mean $\Delta\gamma_{NBP}^{Temp}$, $\Delta\gamma_{NPP}^{Temp}$, and $\Delta\gamma_{Rh}^{Temp}$ values do not show significant changes (Figures S38c and S38f).

Figure S38 shows the correlations of tropical γ_{NBP}^{Temp} with γ_{NPP}^{Temp} and γ_{Rh}^{Temp} during the periods 1955–1979 and 1980–2004 and the correlations of tropical $\Delta\gamma_{NBP}^{Temp}$ with $\Delta\gamma_{NPP}^{Temp}$ and $\Delta\gamma_{Rh}^{Temp}$ during the period 1955–2004 simulated by CMIP5 models. During both periods 1955–1979 and 1980–2004, the significantly negative values of tropical γ_{NBP}^{Temp} in each model (and their average) are explained mainly by the negative values of γ_{NPP}^{Temp}, whereas γ_{Rh}^{Temp} is weakly correlated with γ_{NBP}^{Temp} across models (Figures S38a, S38b, S38d, and S38e). This confirms that the spread of negative tropical γ_{NBP}^{Temp} is mainly due to the suppression of NPP rather than promotion of Rh across CMIP5 models, at least given the current structure of all models.

Most of the CMIP5 ESMs did not capture the observed decrease in apparent sensitivity of tropical NBP to interannual temperature variations in the past five decades (Figure 5b). This may be partly ascribed to the fact that most of the ESMs did not capture the observed regional drying and wetting trends over the last five

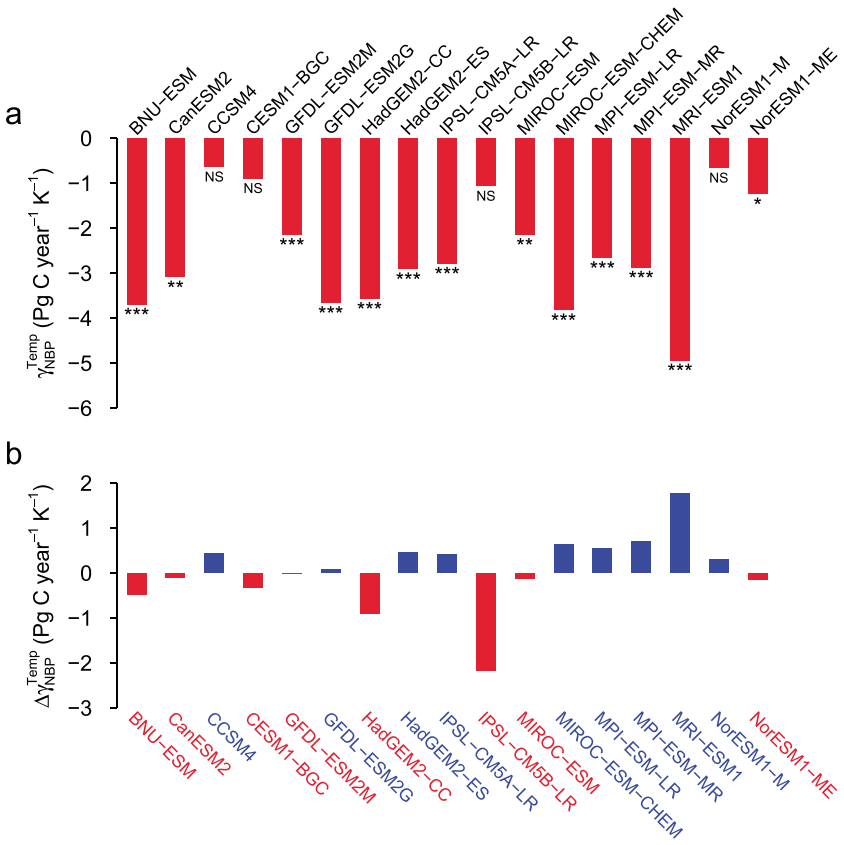

Figure 5. Change in sensitivity of tropical NBP to interannual temperature variations during the period 1955–2004. (a) γ_{NBP}^{Temp} is the sensitivity of tropical NBP to interannual temperature variations for the period 1955–1979 estimated using equation (1). (b) $\Delta\gamma_{NBP}^{Temp}$ is calculated as the difference of γ_{NBP}^{Temp} between the periods 1980–2004 and 1955–1979. Significant differences of γ_{NBP}^{Temp} are reported as NS, $P > 0.05$; *, $P < 0.05$; **, $P < 0.01$; and ***, $P < 0.001$.

decades [*Nasrollahi et al*., 2015]. For instance, during the period 1979–2011, southern Amazonia has experienced a decrease in spring rainfall and an increase in dry season length primarily because of a delay in the end of dry season [*Fu et al*., 2013]. However, the recent changes in both dry season length and the end of dry season were significantly underestimated in CMIP5 ESMs [*Fu et al*., 2013]. Moreover, changes in climate extreme events may contribute to tropical γ_{NBP}^{Temp} changes in the past five decades. However, precipitation extremes in late twentieth century simulated by CMIP5 ESMs are plausible in the extratropics and have very large uncertainties in the tropics and subtropics [*Kharin et al*., 2013]. In addition, many CMIP5 ESMs may underrepresent the processes related to climate-driven forest mortality and its impact on terrestrial carbon cycling [*McDowell et al*., 2011, 2013; *Steinkamp and Hickler*, 2015]. For example, *Brienen et al*. [2015] found that the rates of increase in aboveground biomass of the Amazon rainforest declined over three decades, due to recent leveling off of growth rates and persistent increases of biomass mortality. The long-term increase in mortality rates has yet led to a 30% increase in necromass stocks, because the dead trees decay slowly [*Brienen et al*., 2015]. This indicates that climate-driven forest mortality in tropics probably affects the climate sensitivity of productivity, but may not immediately affect the climate sensitivity of heterotrophic respiration. However, the mechanisms of the observed increase in mortality rates are not accurately represented in CMIP5 ESMs [*Robinson et al*., 2015].

4.2. Interannual Climate Sensitivities of NPP (γ_{NPP}) and Their Changes Over the 21st Century ($\Delta\gamma_{NPP}$)

The simulated sensitivity of NPP to interannual temperature variations is negative in the tropics but positive in boreal regions (Figure 2c). This is expected since the responses of plant photosynthesis to temperature are spatially heterogeneous. In the tropics, ecosystems are near a high-temperature threshold, above which photosynthesis maybe inhibited [*Corlett*, 2011; *Doughty and Goulden*, 2008]. While ecosystems are mainly temperature

limited in boreal regions, where warming can simulate plant photosynthesis [*Wu et al*., 2011] and lead to growing season extension [*Piao et al*., 2007, 2011; *Richardson et al*., 2010]. The photosynthetic response to temperature can be described as a parabolic curve with an optimum temperature, and at temperatures above this optimum, photosynthesis decreases with increasing temperature [*Berry and Björkman*, 1980; *Yamori et al*., 2014] because of an increase in vapor pressure deficit (VPD). Leaf photosynthesis in most ESMs interacts with stomatal conductance [*Shao et al*., 2013]. In terms of the photosynthesis component, stomatal conductance was calculated as a function of relative humidity or VPD varying with different models. When calculating stomatal conductance, relative humidity was used in BNU-ESM, CESM1-BGC, IPSL-CM5A-LR, IPSL-CM5B-LR, and NorESM1-M, and VPD was used in CanESM2, GFDL-ESM2G, GFDL-ESM2M, MPI-ESM-LR, and MPI-ESM-MR [*Wang et al*., 2015].

The interannual climate sensitivity of NPP reflects the combination of short term processes, which itself depends on the background state of the climate and ecosystems. When temperature is lower than the optimal temperature, warming stimulates plant photosynthesis resulting in a positive response of NPP to interannual temperature variability. Under higher temperature, VPD becomes higher and can reduce stomatal conductance and photosynthesis (e.g., gross primary production and NPP). This suggests that the sensitivity of NPP to temperature variations could weaken or become negative if the temperature reaches above the optimum threshold of photosynthesis. Such parabolic temperature response of photosynthesis among C_3 and C_4 plants has been implemented in several vegetation models, as primary components of ESMs (see details in *Smith and Dukes* [2013]). Furthermore, increases in temperature can increase VPD, which reduces NPP and amplifies the negative sensitivity of NPP to temperature variations. Moreover, in response to warming-induced increases in evaporative demand, soil water availability may become limited, which can also suppress the photosynthesis and modulate the NPP sensitivity to temperature variation. The combination of these processes mainly determines how the interannual sensitivity of NPP changes with temperature variations in future climate change. We should inform that CMIP5 models may fail to consider other contributing processes related to the responses of changes in plant expenditure and allocation of carbon assimilates to temperature [*Robinson et al*., 2015]. It is also noteworthy that CMIP5 ESMs do not include temperature acclimation of plant photosynthesis and respiration, which could reduce carbon sensitivity to climate [*Smith et al*., 2015]. For example, when an updated version of CLM (CLM4.5(BGC), version 4.5 of the Community Land Model with active carbon and nitrogen biogeochemical cycling) considering temperature acclimation was run under RCP8.5 climate from CESM (Community Earth System Model), the terrestrial carbon storage increased by 22 PgC by 2100 compared to a model without considering temperature acclimation [*Lombardozzi et al*., 2015].

Compared to the historical reference period (1976–2004), tropical γ_{NPP}^{Temp} is predicted to decrease during 2069–2098 (Figures 1d and 2d). Tropical $\Delta\gamma_{NPP}^{Temp}$ across models decreases with increasing NPP under both RCPs 4.5 and 8.5 (Figures S40d and S42d). This may be related to the possibility that the increase in temperature could be close to or exceed the optimum temperature for photosynthesis in tropical forests. The productivity in tropical forests could then be inhibited due to supraoptimum temperature and/or concurrent increased water limitations. For instance, tropical drought is predicted to become more severe during the 21st century due to either decreased precipitation and/or increased evaporation [*Dai*, 2013]. In boreal regions (e.g., northwestern United States), ESMs predicted higher γ_{NPP}^{Temp} by the end of the 21st century (Figure 2d), probably because temperature is a limiting factor for plant growth in the boreal zone. Warming can stimulate plant photosynthesis and induce growing season extension under RCP8.5 in CMIP5 ESMs [*Maloney et al*., 2014]. In high latitudes, higher NPP is predicted under RCP8.5 in CMIP5 ESMs by the end of the 21st century, due to warming and increasing CO_2 concentration [*Zhao and Zeng*, 2014]. CMIP5 projected NPP shows increase trend during the 21st century at both global and regional scales, but $\Delta\gamma_{NPP}^{Temp}$ was not positively correlated with changes in NPP (ΔNPP) (Figures S39–S42). These indicate that $\Delta\gamma_{NPP}^{Temp}$ was not driven by ΔNPP with a fixed relative magnitude across models but probably by nonlinear response of plant growth to temperature variability.

γ_{NPP}^{Prec} is positive in arid and semiarid regions, e.g., southern United States, central Asia, southern South America, southern African, and Australia (Figure 4c). However, in both the Arctic and the Tibetan Plateau, ESMs show disagreement on the sign of γ_{NPP}^{Prec} (Figure 4c), probably because ecosystems in these cold regions are limited by temperature rather than precipitation. Manipulative ecosystem experiments show that decreased precipitation generally decreases ecosystem productivity, whereas increased precipitation has the opposite effects [*Wu et al*., 2011], yet with possible nonsymmetrical responses [*Unger and Jongen*, 2015]. Note that most of the experiments compiled by *Wu et al*. [2011] were performed in temperate regions

of the Northern Hemisphere, where vegetation is not limited by temperature, but rather by water availability. γ_{NPP}^{Prec} increases in semiarid regions during the 21st century under both RCP4.5 and RCP8.5 (Figures 4d and S20d). For instance, γ_{NPP}^{Prec} shows a significant increase in the temperate bands of the Southern Hemisphere (Figures 3e and 4d), which are predicted over the 21st century [*Collins et al*., 2013; *Dai*, 2013]. This indicates that plant growth in semiarid regions is predicted to become more sensitive to interannual precipitation variations under warmer and drier climatic pathways. Plant growth in semiarid regions is sensitive to precipitation variations, due to water limitation [*Hsu et al*., 2012]. Observations also suggest that the interannual precipitation sensitivity of net carbon uptake in semiarid regions showed a significant increase during the 1982–2011 period, possibly due to expansion of vegetation cover [*Poulter et al*., 2014], increased CO_2 [*Schimel et al*., 2015], or carbon sink anomaly during wet years [*Haverd et al*., 2015].

4.3. Interannual Climate Sensitivities of Rh (γ_{Rh}) and Their Changes Over the 21st Century ($\Delta\gamma_{Rh}$)

γ_{Rh}^{Temp} is mostly positive on a global scale, except in the SH temperate band, where ESMs show disagreement for the sign of interannual temperature sensitivity of Rh (Figure 2e). The Rh variability appears to be positively correlated with interannual precipitation variations globally (Figure 4e). Both generally positive values of γ_{Rh}^{Temp} and γ_{Rh}^{Prec} are due to the positive responses of Rh to temperature and precipitation variations in most ESMs. Rh increases exponentially with temperature in most CMIP5 ESMs, which are usually expressed by functional similar equations: Q_{10} or Arrhenius equations [*Todd-Brown et al*., 2013; *Todd-Brown et al*., 2014]. For example, the Q_{10} equation was used in HadGEM2-ES, HadGEM2-CC, IPSL-CM5A-LR, IPSL-GM5B-LR, and MPI-ESM-LR; the Arrhenius equation was used in BNU-ESM, CCSM4, CESM1-BGC, MIROC-ESM, MIROC-ESM-CHEM, NorESM1-M, and NorEMS1-ME [*Todd-Brown et al*., 2013, 2014]. Decomposition parameterization is a monotonically increasing function of increasing soil moisture in most models (BNU-ESM, CCSM4, CESM1-BGC, GFDL-ESM2G, GFDL-ESM2M, IPSL-CM5A-LR, IPSL-CM5B-LR, MIROC-ESM, MIROC-ESM-CHEM, MPI-ESM-LR, NorESM1-M, and NorESM1-ME) [*Todd-Brown et al*., 2013, 2014]. For example, Rh from each pool is calculated as $Rh \propto kC\, f_r\, f_N\, f_T\, f_w$ in CCSM4, where f_T is based on Q_{10}, and f_w is proportional to soil moisture and the weighting depending on soil water potential [*Shao et al*., 2013]. In ORCHIDEE (Organizing Carbon and Hydrology in Dynamic Ecosystems) coupled to the IPSL-CM4, there is a saturation of f_w at very high soil moisture of 0.5, which is practically never reached [*Krinner et al*., 2005]. Only in CanESM2, HadGEM2-CC, and HadGEM2-ES, decomposition increases up to some optimum moisture level and then decreases [*Todd-Brown et al*., 2013, 2014]. In addition, Rh simulations in current ESMs are mainly based on empirical functions that relate ecohydrologic conditions to decomposition rate of soil organic carbon (SOC) substrates. Decomposition models with reliable microbial-explicit model formulations are recommended to be implemented in next generation of ESMs [*Wieder et al*., 2015].

In boreal regions, predicted multimodel mean γ_{Rh}^{Temp} shows increase trend during the 21st century, possibly due to following two reasons. First, for a fixed amount of SOC, Rh increases exponentially with increasing temperature in most CMIP5 ESMs [*Todd-Brown et al*., 2013, 2014]. Therefore, the magnitude of increase in Rh due to 1 K increase in temperature will be larger during warmer years. During the 21st century period, warming rate in the boreal zone is much higher than that in other regions [*Collins et al*., 2013]. Second, predicted SOC storage at boreal regions shows increasing trend during the 21st century [*Todd-Brown et al*., 2014]. Increased in SOC storage will then lead to an increase in the mean Rh in ESMs [*Exbrayat et al*., 2013; *Shao et al*., 2013; *Todd-Brown et al*., 2013]. Thus, projected increase in SOC available for Rh and the convex (exponential) response of Rh to a unit change of temperature could result in an increase in γ_{Rh}^{Temp} at boreal regions over the 21st century. Compared to the tropics, boreal regions are predicted to experience higher warming rates and larger increases in SOC, both acting to increase the value of γ_{Rh}^{Temp}, especially under RCP8.5 (Figures 2f and S8f–S10f). In addition, we investigated the changes in Rh (ΔRh) during the 21st century and their correlations with $\Delta\gamma_{Rh}^{Temp}$ across models as shown in Figures S39–S42. As expected, both multimodel mean of ΔRh and $\Delta\gamma_{Rh}^{Temp}$ in boreal regions are significantly positive under RCP4.5 and RCP8.5 (Figures S40g and S42g). Across models, the correlations between boreal $\Delta\gamma_{Rh}^{Temp}$ and ΔRh was significant under RCP8.5, but not significant under the other scenarios (Figures S39g–S42g).

Projected 21st century change in mutimodel mean γ_{Rh}^{Prec} is not significant, and there is large spread of $\Delta\gamma_{Rh}^{Prec}$ across models, especially under RCP8.5 (Figures S17, S20f, and S24c). The changes in γ_{Rh}^{Prec} during the 21st century across models are probably due to both monotonic responses of Rh to water condition variations and projected changes in litter and SOC storage. Litter and SOC are critical substrates for

microbial decomposition and therefore influence Rh. For example, under RCP8.5, HadGEM2-ES suggests strong increase in global SOC over the 21st century (253 Pg, 22.6%) due to increase in NPP input [*Todd-Brown et al.*, 2014]. Thus, the HadGEM2-ES produces the largest increase in global γ_{Rh}^{Prec} with $\Delta\gamma_{Rh}^{Prec}$ of 3.01 Pg C yr^{-1} 100 mm^{-1} under RCP8.5 across models (Figures S17 and S24c). Across models, MIROC-ESM suggests the largest decline in global γ_{Rh}^{Prec} with $\Delta\gamma_{Rh}^{Prec}$ of −2.30 Pg C yr^{-1} 100 mm^{-1} under RCP8.5 (Figures S17 and S24c), likely due to its strong decrease in global SOC over the 21st century (−72 Pg, −2.8%) [*Todd-Brown et al.*, 2014].

4.4. Interannual Climate Sensitivities of NBP (γ_{NBP}) and Their Changes Over the 21st Century ($\Delta\gamma_{NBP}$)

γ_{NBP}^{Temp} (γ_{NBP}^{Prec}) is determined by interannual temperature (precipitation) sensitivities of both NPP and Rh. In boreal regions, the magnitudes of γ_{NPP}^{Temp} and γ_{Rh}^{Temp} are comparable in ESMs, resulting in insignificant γ_{NBP}^{Temp}. However, in the tropics, NBP negatively responds to interannual temperature variations, probably due to the negative γ_{NPP}^{Temp} and positive γ_{Rh}^{Temp}. The absolute magnitude of γ_{Rh}^{Prec} is suggested to be lower than that of γ_{NPP}^{Prec} in many regions except for the boreal regions (Figures 4c and 4e), resulting in a positive value of γ_{NBP}^{Prec} in tropical and temperate regions (Figure 4a). This is consistent with observations of manipulative experiments in temperate ecosystems, where increased precipitation led to a greater increase in NPP than Rh resulting in increased net carbon uptake (i.e., NBP) [*Wu et al.*, 2011]. This suggests that vegetation productivity is more sensitive to precipitation variations than soil respiration, due to their difference responses. For example, in grassland ecosystems across the Great Plains in USA, the response of NPP to drought variation is attributable to rainfall amount, but drought impacts Rh by a relatively slower process, e.g., soil drying, reduced carbon input, and a drought-induced reduction in soil carbon content [*Shi et al.*, 2014].

Changes in global γ_{NBP}^{Temp} (γ_{NBP}^{Prec}) over the 21th century are determined by both changes in γ_{NPP}^{Temp} (γ_{NPP}^{Prec}) and γ_{Rh}^{Temp} (γ_{Rh}^{Prec}). Under RCP4.5, at global scale, different influences of $\Delta\gamma_{NPP}^{Temp}$ and $\Delta\gamma_{Rh}^{Temp}$ on $\Delta\gamma_{NBP}^{Temp}$ are predicted to nearly cancel each other out, leading to nonsignificant change in γ_{NBP}^{Temp}. But this result is not consistent across all RCPs. For example, under RCP8.5, global γ_{NBP}^{Temp} is found to decrease, due to a decrease in tropical γ_{NPP}^{Temp} and an increase of γ_{Rh}^{Temp} in extratropical regions (Figures S7 and S10). Over the 21st century, the response of NBP to interannual precipitation variations in the ESMs remains relatively stable globally under RCP4.5 (Figure 4b). However, under RCP8.5, γ_{NBP}^{Prec} increases significantly in the central United States, the central Asia, and the southern Australia (Figure S20b), where semiarid ecosystems are widely distributed. The increased γ_{NBP}^{Prec} in these regions is probably caused by changes in γ_{NPP}^{Prec} rather than changes in γ_{Rh}^{Prec}. Besides semiarid regions, tropical ecosystem carbon cycles are also sensitive to precipitation variations [*Gatti et al.*, 2014]. The reduction of precipitation since 2000 has led to a decline in vegetation greenness across large parts of Amazonia [*Hilker et al.*, 2014]. In the anomalously dry year 2010, Amazonian forest became carbon neutral, primarily resulting from the suppression of photosynthesis during drought [*Gatti et al.*, 2014]. The positive relationship between NBP and precipitation variability on the interannual timescale in tropical regions seems to be captured by the ESMs (Figure 4a). However, although tropics becomes drier by the end of the 21st century under RCP4.5 pathway [*Collins et al.*, 2013; *Dai*, 2013], tropical γ_{NBP}^{Prec} remains relatively stable in the ESMs over the 21st century (Figures 3d and 4b), perhaps partly due to CO_2 increases. Among all models, only MIROC-ESM predicts a relatively large increase of tropical γ_{NBP}^{Prec} under RCP4.5, mainly due to a large decrease of γ_{Rh}^{Prec}, but not change in γ_{NPP}^{Prec} (Figures 3d and 3i).

4.5. Uncertainty of Projection in Interannual Climate Sensitivities of Carbon Fluxes Simulated by CMIP5 ESMs

The responses of terrestrial carbon fluxes to interannual temperature and precipitation variations show large spreads across models, leading to uncertainties in their future projections. Several key biogeochemical processes (e.g., nutrient limitation, permafrost dynamics, and microbial decomposition) are recommended to be represented in the ESMs to improve their terrestrial carbon fluxes responses to climate change. First, C-N interactions would affect the terrestrial carbon cycle response to temperature and precipitation variations [*Thornton et al.*, 2007]. For instance, when atmospheric CO_2 concentration rises, the carbon cycle responses to temperature and precipitation variation increase in magnitude for the carbon-only model of CLM 3.0 but are reduced in magnitude for the coupled C-N model of CLM-CN [*Thornton et al.*, 2007]. If nitrogen constraint on carbon cycling was considered, land carbon sequestration simulated by CMIP5 ESMs between 1860 and

2100 could decrease by between 97 Pg C (RCP 2.6) and 150 Pg C (RCP 8.5) [*Zaehle et al*., 2015]. However, in CMIP5 simulations, C-N interactions was incorporated in the simulations of only two ESMs: CESM1-BGC and NorESM1-ME, both of which used CLM as the surface model and had a relatively weak carbon-climate feedbacks [*Arora et al*., 2013]. Under RCP4.5, global $\Delta\gamma_{NBP}^{Temp}$ is 2.07 Pg C year^{-1} K^{-1} in NorESM1-ME with N cycle and −1.27 Pg C year^{-1} K^{-1} in NorESM1-M without N cycle (Figure 1a). Here note that besides the N cycle, ocean biogeochemistry (HAMOCC5) has been implemented in NorESM1-ME, but not in NorESM1-M [*Tjiputra et al*., 2013]. Second, Arctic terrestrial ecosystems, containing huge organic carbon stock, are sensitive to climate change [*Koven et al*., 2015; *McGuire et al*., 2009; *Schuur et al*., 2015; *Tarnocai et al*., 2009]. Warming cannot only accelerate ecosystem productivity in Arctic regions but also result in the acceleration of permafrost soil carbon decomposition [*Koven et al*., 2011; *Schuur et al*., 2008]. Permafrost soil carbon will have a positive feedback to global climate change, when carbon losses due to respiration exceed carbon gains through increase NPP. The permafrost carbon sensitivities are poorly represented in most ESMs, which lead to large predicted SOC change uncertainty [*Todd-Brown et al*., 2014], resulting uncertainty in prediction of changes in Rh apparent sensitivity to interannual temperature variations over the 21st century. Third, Q_{10} function or Arrhenius equation expresses the relationship between Rh and temperature in most CMIP5 ESMs [*Shao et al*., 2013]. However, the temperature sensitivity of decomposition (Q_{10}) can be directly and indirectly affected by environmental factors, e.g., temperature, soil moisture, and substrate quality [*Davidson and Janssens*, 2006; *Davidson et al*., 2006; *Exbrayat et al*., 2013; *Tang and Riley*, 2015]. For example, temperature sensitivity of soil respiration in boreal and Arctic soil is higher than that in other regions [*Karhu et al*., 2014]. Microbes included in soil carbon models can change the sign of the response of soil carbon to warming. It simulates an accumulation of soil carbon if microbial growth efficiency declines with warming, but a large carbon loss if the adaptation of growth efficiency to warming is allowed [*Wieder et al*., 2013, 2014]. Despite of this, in most CMIP5 ESMs, Q_{10} is parameterized as a constant value under future climate change scenarios.

5. Conclusions

In this paper, the simulations of CMIP5 Earth System Models (ESMs) have been analyzed, focusing on the changes in response of terrestrial carbon fluxes to interannual temperature, precipitation, and radiation variations under historical scenario (1975–2004) and under the four RCPs (2069–2098). We analyzed here the changes in the apparent sensitivities of net biome production (NBP), net primary production (NPP), and heterotrophic respiration (Rh) to interannual variations in temperature (γ^{Temp}), precipitation (γ^{Prec}), and radiation (γ^{Radi}) over the 21st century ($\Delta\gamma^{Temp}$, $\Delta\gamma^{Prec}$, and $\Delta\gamma^{Radi}$) at both global and regional scales.

Most ESMs predict a decrease of γ_{NBP}^{Temp} in the tropics by the end of the 21st century, probably due to warming (above optimum temperature of photosynthesis) and severe drought [*Dai*, 2013; *Feng and Fu*, 2013; *Orlowsky and Seneviratne*, 2013; *Scheff and Frierson*, 2015]. However, most ESMs do not capture the observed decrease in tropical γ_{NBP}^{Temp} during the past five decades, mainly because the observed long-term (1950–2005) regional drying and wetting trends was not captured in most ESMs [*Nasrollahi et al*., 2015]. To capture the correct changes in terrestrial γ_{NBP}^{Temp}, we recommend to improve model's ability to simulate regional wetting/drying trends unless which are caused by internal variability.

High northern latitude regions are predicted to experience an increase of γ_{Rh}^{Temp} in most ESMs during the 21st century, which can be ascribed to high warming rates and large increases in soil organic carbon [*Todd-Brown et al*., 2014]. However, this merits further investigation since current state-of-the-art ESMs do not consider the large quantities of organic carbon stored in frozen soils in Arctic and sub-Arctic regions [*Todd-Brown et al*., 2014]. In the future warming climate, there may be a gradual and prolonged release of carbon dioxide from this inert carbon pool, which can exceed warming-induced increase in NPP and result in a net carbon loss over the regions underlaid by permafrost [*Koven et al*., 2011; *Schuur et al*., 2008, 2015].

Modeled γ_{NPP}^{Prec} shows an increased trend in central United States, central Asia, and southern Australia during the 21st century, like observed over the last three decades in *Poulter et al*. [2014]. In semiarid regions such as Australia, the sensitivity of net carbon uptake to precipitation was found to have increased in the last three decades, probably due to changes in ecosystem productivity caused by expansion of vegetation cover [*Poulter et al*., 2014], increased CO_2 [*Schimel et al*., 2015], or carbon sink anomaly during wet years [*Haverd et al*., 2015]. However, in the temperate band of Southern Hemisphere, the multimodel mean γ_{NBP}^{Prec} remains relatively stable with a large model spread. Moreover, most ESMs captured the positive relation between

NBP and interannual precipitation variability in tropical regions over the past five decades. However, tropical γ_{NBP}^{Prec} remains relative stable across ESMs in the future, although tropics become drier by the end of the 21st century under RCP4.5 pathway [*Collins et al*., 2013; *Dai*, 2013].

Across most of ESMs, differences in the changes in interannual climate sensitivities of NBP can be mainly explained by that of NPP rather than that of Rh. There are large uncertainties in the future projections of the responses of terrestrial carbon fluxes to interannual climate variations. To capture the plausible changes in land carbon fluxes sensitivities to climate change, several key biogeochemical processes, e.g., C-N interactions, permafrost dynamics, soil moisture optimum, and microbial decomposition, are thus recommended to be incorporated or improved in next generation of ESMs.

Acknowledgments
This study was supported by the National Natural Science Foundation of China (41125004), Chinese Ministry of Environmental Protection grant (201209031), and National Youth Top-notch Talent Support Program in China. The outputs of CMIP5 ESMs were downloaded from the Program for Climate Model Diagnosis and Intercomparison (PCMDI) server: Earth System Grid Federation (http://cmip-pcmdi.llnl.gov/cmip5). The NDVI data were obtained from the Global Inventory Monitoring and Modelling Studies (GIMMS) group. The authors acknowledge the three anonymous reviewers for their constructive comments that greatly improved the manuscript.

References

Ahlström, A., et al. (2015), The dominant role of semi-arid ecosystems in the trend and variability of the land CO_2 sink, *Science*, *348*(6237), 895–899, doi:10.1126/science.aaa1668.

Angert, A., S. Biraud, C. Bonfils, C. C. Henning, W. Buermann, J. Pinzon, C. J. Tucker, and I. Fung (2005), Drier summers cancel out the CO_2 uptake enhancement induced by warmer springs, *Proc. Natl. Acad. Sci. U.S.A.*, *102*(31), 10,823–10,827, doi:10.1073/pnas.0501647102.

Arora, V. K., et al. (2013), Carbon-concentration and carbon-climate feedbacks in CMIP5 Earth System Models, *J. Clim.*, *26*(15), 5289–5314, doi:10.1175/Jcli-D-12-00494.1.

Bastos, A., S. W. Running, C. Gouveia, and R. M. Trigo (2013), The global NPP dependence on ENSO: La Nina and the extraordinary year of 2011, *J. Geophys. Res. Biogeosci.*, *118*, 1247–1255, doi:10.1002/jgrg.20100.

Berry, J., and O. Björkman (1980), Photosynthetic response and adaptation to temperature in higher plants, *Annu. Rev. Plant Phys.*, *31*, 491–543, doi:10.1146/annurev.pp.31.060180.002423.

Bond-Lamberty, B., and A. Thomson (2010), Temperature-associated increases in the global soil respiration record, *Nature*, *464*(7288), 579–582, doi:10.1038/Nature08930.

Brienen, R. J. W., et al. (2015), Long-term decline of the Amazon carbon sink, *Nature*, *519*(7543), 344–348, doi:10.1038/nature14283.

Cinquini, L., et al. (2014), The Earth System Grid Federation: An open infrastructure for access to distributed geospatial data, *Future Gener. Comput. Syst.*, *36*, 400–417, doi:10.1016/j.future.2013.07.002.

Collins, M., et al. (2013), Long-term climate change: Projections, commitments and irreversibility, in *Climate change 2013: The Physical Science Basis. Contribution of Working Group I to the Fifth Assessment Report of the Intergovernmental Panel on Climate Change*, edited by T. F. Stocker et al., pp. 1029–1136, Cambridge Univ. Press, Cambridge, U. K., and New York.

Corlett, R. T. (2011), Impacts of warming on tropical lowland rainforests, *Trends Ecol. Evol.*, *26*(11), 606–613, doi:10.1016/j.tree.2011.06.015.

Cox, P. M., R. A. Betts, M. Collins, P. P. Harris, C. Huntingford, and C. D. Jones (2004), Amazonian forest dieback under climate-carbon cycle projections for the 21st century, *Theor. Appl. Climatol.*, *78*(1-3), 137–156, doi:10.1007/s00704-004-0049-4.

Cox, P. M., D. Pearson, B. B. Booth, P. Friedlingstein, C. Huntingford, C. D. Jones, and C. M. Luke (2013), Sensitivity of tropical carbon to climate change constrained by carbon dioxide variability, *Nature*, *494*(7437), 341–344, doi:10.1038/Nature11882.

Dai, A. G. (2013), Increasing drought under global warming in observations and models, *Nat. Clim. Change*, *3*(1), 52–58, doi:10.1038/Nclimate1633.

Davidson, E. A., and I. A. Janssens (2006), Temperature sensitivity of soil carbon decomposition and feedbacks to climate change, *Nature*, *440*(7081), 165–173, doi:10.1038/Nature04514.

Davidson, E. A., I. A. Janssens, and Y. Q. Luo (2006), On the variability of respiration in terrestrial ecosystems: Moving beyond Q_{10}, *Global Change Biol.*, *12*(2), 154–164, doi:10.1111/j.1365-2486.2005.01065.x.

Doughty, C. E., and M. L. Goulden (2008), Are tropical forests near a high temperature threshold?, *J. Geophys. Res.*, *113*, G00B07, doi:10.1029/2007JG000632.

Exbrayat, J. F., A. J. Pitman, Q. Zhang, G. Abramowitz, and Y. P. Wang (2013), Examining soil carbon uncertainty in a global model: Response of microbial decomposition to temperature, moisture and nutrient limitation, *Biogeosciences*, *10*(11), 7095–7108, doi:10.5194/bg-10-7095-2013.

Feng, S., and Q. Fu (2013), Expansion of global drylands under a warming climate, *Atmos. Chem. Phys.*, *13*(19), 10,081–10,094, doi:10.5194/acp-13-10081-2013.

Fu, R., et al. (2013), Increased dry-season length over southern Amazonia in recent decades and its implication for future climate projection, *Proc. Natl. Acad. Sci. U.S.A.*, *110*(45), 18,110–18,115, doi:10.1073/pnas.1302584110.

Gatti, L. V., et al. (2014), Drought sensitivity of Amazonian carbon balance revealed by atmospheric measurements, *Nature*, *506*(7486), 76–80, doi:10.1038/Nature12957.

Guenet, B., F. E. Moyano, N. Vuichard, G. J. D. Kirk, P. H. Bellamy, S. Zaehle, and P. Ciais (2013), Can we model observed soil carbon changes from a dense inventory? A case study over England and Wales using three versions of the ORCHIDEE ecosystem model (AR5, AR5-PRIM and O-CN), *Geosci. Model Dev.*, *6*(6), 2153–2163, doi:10.5194/gmd-6-2153-2013.

Haverd, V., B. Smith, and C. Trudinger (2015), Dryland vegetation response to wet episode, not inherent shift in sensitivity to rainfall, behind Australia's role in 2011 global carbon sink anomaly, *Global Change Biol.*, doi:10.1111/gcb.13202.

Hilker, T., A. I. Lyapustin, C. J. Tucker, F. G. Hall, R. B. Myneni, Y. J. Wang, J. Bi, Y. M. de Moura, and P. J. Sellers (2014), Vegetation dynamics and rainfall sensitivity of the Amazon, *Proc. Natl. Acad. Sci. U.S.A.*, *111*(45), 16,041–16,046, doi:10.1073/pnas.1404870111.

Hsu, J. S., J. Powell, and P. B. Adler (2012), Sensitivity of mean annual primary production to precipitation, *Global Change Biol.*, *18*(7), 2246–2255, doi:10.1111/j.1365-2486.2012.02687.x.

Ji, D., et al. (2014), Description and basic evaluation of Beijing Normal University Earth System Model (BNU-ESM) version 1, *Geosci. Model Dev.*, *7*(5), 2039–2064, doi:10.5194/gmd-7-2039-2014.

Jones, C., et al. (2013), Twenty-first-century compatible CO_2 emissions and airborne fraction simulated by CMIP5 Earth System Models under four representative concentration pathways, *J. Clim.*, *26*(13), 4398–4413, doi:10.1175/Jcli-D-12-00554.1.

Jones, P. W. (1999), First- and second-order conservative remapping schemes for grids in spherical coordinates, *Mon. Weather Rev.*, *127*(9), 2204–2210, doi:10.1175/1520-0493(1999)127<2204:Fasocr>2.0.Co;2.

Karhu, K., et al. (2014), Temperature sensitivity of soil respiration rates enhanced by microbial community response, *Nature*, *513*(7516), 81–84, doi:10.1038/Nature13604.
Kharin, V. V., F. W. Zwiers, X. Zhang, and M. Wehner (2013), Changes in temperature and precipitation extremes in the CMIP5 ensemble, *Clim. Change*, *119*(2), 345–357, doi:10.1007/s10584-013-0705-8.
Koven, C. D., B. Ringeval, P. Friedlingstein, P. Ciais, P. Cadule, D. Khvorostyanov, G. Krinner, and C. Tarnocai (2011), Permafrost carbon-climate feedbacks accelerate global warming, *Proc. Natl. Acad. Sci. U.S.A.*, *108*(36), 14,769–14,774, doi:10.1073/pnas.1103910108.
Koven, C. D., D. M. Lawrence, and W. J. Riley (2015), Permafrost carbon−climate feedback is sensitive to deep soil carbon decomposability but not deep soil nitrogen dynamics, *Proc. Natl. Acad. Sci. U.S.A.*, *112*(12), 3752–3757, doi:10.1073/pnas.1415123112.
Krinner, G., N. Viovy, N. de Noblet-Ducoudre, J. Ogee, J. Polcher, P. Friedlingstein, P. Ciais, S. Sitch, and I. C. Prentice (2005), A dynamic global vegetation model for studies of the coupled atmosphere-biosphere system, *Global Biogeochem. Cycles*, *19*, GB1015, doi:10.1029/2003GB002199.
Lombardozzi, D. L., G. B. Bonan, N. G. Smith, J. S. Dukes, and R. A. Fisher (2015), Temperature acclimation of photosynthesis and respiration: A key uncertainty in the carbon cycle-climate feedback, *Geophys. Res. Lett.*, *42*, 8624–8631, doi:10.1002/2015GL065934.
Maloney, E. D., et al. (2014), North American climate in CMIP5 experiments: Part III: Assessment of twenty-first-century projections, *J. Clim.*, *27*(6), 2230–2270, doi:10.1175/Jcli-D-13-00273.1.
Masui, T., K. Matsumoto, Y. Hijioka, T. Kinoshita, T. Nozawa, S. Ishiwatari, E. Kato, P. R. Shukla, Y. Yamagata, and M. Kainuma (2011), An emission pathway for stabilization at 6 W m^{-2} radiative forcing, *Clim. Change*, *109*(1-2), 59–76, doi:10.1007/s10584-011-0150-5.
McDowell, N. G., D. J. Beerling, D. D. Breshears, R. A. Fisher, K. F. Raffa, and M. Stitt (2011), The interdependence of mechanisms underlying climate-driven vegetation mortality, *Trends Ecol. Evol.*, *26*(10), 523–532, doi:10.1016/j.tree.2011.06.003.
McDowell, N. G., M. G. Ryan, M. J. B. Zeppel, and D. T. Tissue (2013), Improving our knowledge of drought-induced forest mortality through experiments, observations, and modeling, *New Phytol.*, *200*(2), 289–293, doi:10.1111/nph.12502.
McGuire, A. D., L. G. Anderson, T. R. Christensen, S. Dallimore, L. D. Guo, D. J. Hayes, M. Heimann, T. D. Lorenson, R. W. Macdonald, and N. Roulet (2009), Sensitivity of the carbon cycle in the Arctic to climate change, *Ecol. Monogr.*, *79*(4), 523–555, doi:10.1890/08-2025.1.
Nasrollahi, N., A. AghaKouchak, L. Cheng, L. Damberg, T. J. Phillips, C. Miao, K. Hsu, and S. Sorooshian (2015), How well do CMIP5 climate simulations replicate historical trends and patterns of meteorological droughts? *Water Resour. Res.*, *51*, 2847–2864, doi:10.1002/2014WR016318.
Orlowsky, B., and S. I. Seneviratne (2013), Elusive drought: Uncertainty in observed trends and short- and long-term CMIP5 projections, *Hydrol. Earth Syst. Sci.*, *17*(5), 1765–1781, doi:10.5194/hess-17-1765-2013.
Piao, S. L., P. Friedlingstein, P. Ciais, N. Viovy, and J. Demarty (2007), Growing season extension and its impact on terrestrial carbon cycle in the Northern Hemisphere over the past 2 decades, *Global Biogeochem. Cycles*, *21*, GB3018, doi:10.1029/2006GB002888.
Piao, S. L., X. H. Wang, P. Ciais, B. Zhu, T. Wang, and J. Liu (2011), Changes in satellite-derived vegetation growth trend in temperate and boreal Eurasia from 1982 to 2006, *Global Change Biol.*, *17*(10), 3228–3239, doi:10.1111/j.1365-2486.2011.02419.x.
Piao, S. L., et al. (2013), Evaluation of terrestrial carbon cycle models for their response to climate variability and to CO_2 trends, *Global Change Biol.*, *19*(7), 2117–2132, doi:10.1111/Gcb.12187.
Piao, S. L., et al. (2014), Evidence for a weakening relationship between interannual temperature variability and northern vegetation activity, *Nat. Commun.*, *5*, doi:10.1038/Ncomms6018.
Pinzon, J. E., and C. J. Tucker (2014), A non-stationary 1981-2012 AVHRR NDVI3g time series, *Remote Sens.*, *6*(8), 6929–6960, doi:10.3390/rs6086929.
Poulter, B., et al. (2013), Recent trends in Inner Asian forest dynamics to temperature and precipitation indicate high sensitivity to climate change, *Agric. For. Meteorol.*, *178*, 31–45, doi:10.1016/j.agrformet.2012.12.006.
Poulter, B., et al. (2014), Contribution of semi-arid ecosystems to interannual variability of the global carbon cycle, *Nature*, *509*(7502), 600–603, doi:10.1038/Nature13376.
Riahi, K., S. Rao, V. Krey, C. H. Cho, V. Chirkov, G. Fischer, G. Kindermann, N. Nakicenovic, and P. Rafaj (2011), RCP 8.5-A scenario of comparatively high greenhouse gas emissions, *Clim. Change*, *109*(1-2), 33–57, doi:10.1007/s10584-011-0149-y.
Richardson, A. D., et al. (2010), Influence of spring and autumn phenological transitions on forest ecosystem productivity, *Philos. Trans. R. Soc. B*, *365*(1555), 3227–3246, doi:10.1098/rstb.2010.0102.
Robinson, I. N.-J., D. K. Charles, J. R. William, G. K. Ryan, and Q. C. Jeffrey (2015), Observed allocations of productivity and biomass, and turnover times in tropical forests are not accurately represented in CMIP5 Earth System Models, *Environ. Res. Lett.*, *10*(6), 064017, doi:10.1088/1748-9326/10/6/064017.
Scheff, J., and D. M. W. Frierson (2015), Terrestrial aridity and its response to greenhouse warming across CMIP5 climate models, *J. Clim.*, *28*, 5583–5600, doi:10.1175/JCLI-D-14-00480.1.
Schimel, D., B. B. Stephens, and J. B. Fisher (2015), Effect of increasing CO_2 on the terrestrial carbon cycle, *Proc. Natl. Acad. Sci. U.S.A.*, *112*(2), 436–441, doi:10.1073/pnas.1407302112/-/DCSupplemental.
Schneising, O., M. Reuter, M. Buchwitz, J. Heymann, H. Bovensmann, and J. P. Burrows (2014), Terrestrial carbon sink observed from space: Variation of growth rates and seasonal cycle amplitudes in response to interannual surface temperature variability, *Atmos. Chem. Phys.*, *14*(1), 133–141, doi:10.5194/acp-14-133-2014.
Schuur, E. A. G., et al. (2008), Vulnerability of permafrost carbon to climate change: Implications for the global carbon cycle, *BioScience*, *58*(8), 701–714, doi:10.1641/B580807.
Schuur, E. A. G., et al. (2015), Climate change and the permafrost carbon feedback, *Nature*, *520*(7546), 171–179, doi:10.1038/nature14338.
Shao, P., X. B. Zeng, D. J. P. Moore, and X. D. Zeng (2013), Soil microbial respiration from observations and Earth System Models, *Environ. Res. Lett.*, *8*(3, 034034), doi:10.1088/1748-9326/8/3/034034.
Shi, Z., M. L. Thomey, W. Mowll, M. Litvak, N. A. Brunsell, S. L. Collins, W. T. Pockman, M. D. Smith, A. K. Knapp, and Y. Luo (2014), Differential effects of extreme drought on production and respiration: Synthesis and modeling analysis, *Biogeosciences*, *11*(3), 621–633, doi:10.5194/bg-11-621-2014.
Smith, N. G., and J. S. Dukes (2013), Plant respiration and photosynthesis in global-scale models: Incorporating acclimation to temperature and CO_2, *Global Change Biol.*, *19*(1), 45–63, doi:10.1111/j.1365-2486.2012.02797.x.
Smith, N. G., S. L. Malyshev, E. Shevliakova, J. Kattge, and J. S. Dukes (2015), Foliar temperature acclimation reduces simulated carbon sensitivity to climate, *Nat. Clim. Change*, doi:10.1038/nclimate2878.
Steinkamp, J., and T. Hickler (2015), Is drought-induced forest dieback globally increasing?, *J. Ecol.*, *103*(1), 31–43, doi:10.1111/1365-2745.12335.
Tang, J. Y., and W. J. Riley (2015), Weaker soil carbon-climate feedbacks resulting from microbial and abiotic interactions, *Nat. Clim. Change*, *5*(1), 56–60, doi:10.1038/Nclimate2438.
Tarnocai, C., J. G. Canadell, E. A. G. Schuur, P. Kuhry, G. Mazhitova, and S. Zimov (2009), Soil organic carbon pools in the northern circumpolar permafrost region, *Global Biogeochem. Cycles*, *23*, GB2023, doi:10.1029/2008GB003327.
Taylor, K. E., R. J. Stouffer, and G. A. Meehl (2012), An overview of CMIP5 and the experiment design, *Bull. Am. Meteorol. Soc.*, *93*(4), 485–498, doi:10.1175/Bams-D-11-00094.1.

Thomson, A. M., et al. (2011), RCP4.5: A pathway for stabilization of radiative forcing by 2100, *Clim. Change*, *109*(1-2), 77–94, doi:10.1007/s10584-011-0151-4.

Thornton, P. E., J. F. Lamarque, N. A. Rosenbloom, and N. M. Mahowald (2007), Influence of carbon-nitrogen cycle coupling on land model response to CO_2 fertilization and climate variability, *Global Biogeochem. Cycles*, *21*, GB4018, doi:10.1029/2006GB002868.

Tjiputra, J. F., C. Roelandt, M. Bentsen, D. M. Lawrence, T. Lorentzen, J. Schwinger, O. Seland, and C. Heinze (2013), Evaluation of the carbon cycle components in the Norwegian Earth System Model (NorESM), *Geosci. Model Dev.*, *6*(2), 301–325, doi:10.5194/gmd-6-301-2013.

Todd-Brown, K. E. O., J. T. Randerson, W. M. Post, F. M. Hoffman, C. Tarnocai, E. A. G. Schuur, and S. D. Allison (2013), Causes of variation in soil carbon simulations from CMIP5 Earth System Models and comparison with observations, *Biogeosciences*, *10*(3), 1717–1736, doi:10.5194/bg-10-1717-2013.

Todd-Brown, K. E. O., et al. (2014), Changes in soil organic carbon storage predicted by Earth System Models during the 21st century, *Biogeosciences*, *11*(8), 2341–2356, doi:10.5194/bg-11-2341-2014.

Unger, S., and M. Jongen (2015), Consequences of changing precipitation patterns for ecosystem functioning in grasslands: A review, in *Progress in Botany*, vol. 76, edited by U. Lüttge and W. Beyschlag, pp. 347–393, Springer Int. Publishing, Switzerland.

van der Werf, G. R., J. T. Randerson, L. Giglio, G. J. Collatz, M. Mu, P. S. Kasibhatla, D. C. Morton, R. S. DeFries, Y. Jin, and T. T. van Leeuwen (2010), Global fire emissions and the contribution of deforestation, savanna, forest, agricultural, and peat fires (1997–2009), *Atmos. Chem. Phys.*, *10*(23), 11,707–11,735, doi:10.5194/acp-10-11707-2010.

van Vuuren, D. P., et al. (2011a), RCP2.6: Exploring the possibility to keep global mean temperature increase below 2°C, *Clim. Change*, *109*(1-2), 95–116, doi:10.1007/s10584-011-0152-3.

van Vuuren, D. P., et al. (2011b), The representative concentration pathways: An overview, *Clim. Change*, *109*(1-2), 5–31, doi:10.1007/s10584-011-0148-z.

Wang, T., X. Lin, Y. Liu, S. Dantec-Nédélec, and C. Ottlé (2015), Causes of uncertainty in China's net primary production over the 21st century projected by the CMIP5 Earth System Models, *Int. J. Climatol.*, doi:10.1002/joc.4497.

Wang, X. H., et al. (2014), A two-fold increase of carbon cycle sensitivity to tropical temperature variations, *Nature*, *506*(7487), 212–215, doi:10.1038/Nature12915.

Wenzel, S., P. M. Cox, V. Eyring, and P. Friedlingstein (2014), Emergent constraints on climate-carbon cycle feedbacks in the CMIP5 Earth System Models, *J. Geophys. Res. Biogeosci.*, *119*, 794–807, doi:10.1002/2013JG002591.

Wieder, W. R., G. B. Bonan, and S. D. Allison (2013), Global soil carbon projections are improved by modelling microbial processes, *Nat. Clim. Change*, *3*(10), 909–912, doi:10.1038/Nclimate1951.

Wieder, W. R., A. S. Grandy, C. M. Kallenbach, and G. B. Bonan (2014), Integrating microbial physiology and physio-chemical principles in soils with the MIcrobial-MIneral Carbon Stabilization (MIMICS) model, *Biogeosciences*, *11*(14), 3899–3917, doi:10.5194/bg-11-3899-2014.

Wieder, W. R., et al. (2015), Explicitly representing soil microbial processes in Earth System Models, *Global Biogeochem. Cycles*, *29*, 1782–1800, doi:10.1002/2015GB005188.

Wu, Z. T., P. Dijkstra, G. W. Koch, J. Penuelas, and B. A. Hungate (2011), Responses of terrestrial ecosystems to temperature and precipitation change: A meta-analysis of experimental manipulation, *Global Change Biol.*, *17*(2), 927–942, doi:10.1111/j.1365-2486.2010.02302.x.

Yamori, W., K. Hikosaka, and D. A. Way (2014), Temperature response of photosynthesis in C_3, C_4, and CAM plants: Temperature acclimation and temperature adaptation, *Photosynth. Res.*, *119*(1-2), 101–117, doi:10.1007/s11120-013-9874-6.

Zaehle, S., C. D. Jones, B. Houlton, J. F. Lamarque, and E. Robertson (2015), Nitrogen availability reduces CMIP5 projections of twenty-first-century land carbon uptake, *J. Clim.*, *28*(6), 2494–2511, doi:10.1175/Jcli-D-13-00776.1.

Zeng, N., A. Mariotti, and P. Wetzel (2005), Terrestrial mechanisms of interannual CO_2 variability, *Global Biogeochem. Cycles*, *19* GB1016, doi:10.1029/2004GB0022763.

Zhao, F., and N. Zeng (2014), Continued increase in atmospheric CO_2 seasonal amplitude in the 21st century projected by the CMIP5 Earth System Models, *Earth Syst. Dyn.*, *5*(2), 423–439, doi:10.5194/esd-5-423-2014.